CMB anisotropy at degree angular scales and the thermal history of the Universe

Paolo de Bernardis

Dipartimento di Fisica, Università di Roma La Sapienza

P.le A. Moro 2, 00185 Roma, Italy.

e-mail: debernardis@roma1.infn.it

Amedeo Balbi, Giancarlo De Gasperis

Dipartimento di Fisica, Universitá di Roma Tor Vergata

Via della Ricerca Scientifica, 00133 Roma, Italy

e-mail: balbi@roma2.infn.it, degasperis@roma2.infn.it,

Alessandro Melchiorri

Dipartimento di Fisica, Università di Roma La Sapienza

P.le A. Moro 2, 00185 Roma, Italy.

e-mail: melchiorria@roma1.infn.it

Nicola Vittorio

Dipartimento di Fisica, Universitá di Roma Tor Vergata

Via della Ricerca Scientifica, 00133 Roma, Italy

e-mail: vittorio@roma2.infn.it

Received _____; accepted _____

Submitted to ApJ

ABSTRACT

We study the anisotropy of the cosmic microwave background (CMB) in cold and mixed dark matter (CDM and MDM) models, with non scale-invariant primordial power spectra (i.e. $n \neq 1$) and a late, sudden reionization of the intergalactic medium at redshift z_{rh}. We test these models against recent detections of CMB anisotropy at large and intermediate angular scales. We find that current CMB anisotropy measurements cannot discriminate between CDM and MDM models. Our likelihood analysis indicates that models with blue power spectra ($n \simeq 1.2$) and a reionization at $z_{rh} \sim 20$ are most consistent with the anisotropy data considered here. Without reionization our analysis gives $1.0 \leq n \leq 1.26$ (95% C.L.) for $\Omega_b = 0.05$.

Subject headings: cosmic microwave background - dark matter - galaxies: formation.

1. Introduction

The COBE/DMR experiment (Smoot et al. 1992) has revolutionized the field of structure formation, providing the first robust evidence for primary, large scale anisotropy of the cosmic microwave background (CMB). On these angular scales CMB anisotropies are expected because of potential fluctuations at last scattering (Sachs & Wolfe 1967). These linear fluctuations are predicted to be constant in time, and then provide a unique tool for determining the initial conditions out of which large scale structure formed. Because of the low COBE/DMR angular resolution and of the correspondingly large cosmic variance (Abbot & Wise,1984), these initial conditions can not be yet determined with high precision (Scaramella & Vittorio 1993, Bennet et al., 1994). In spite of this, scale-invariant initial conditions, a robust prediction of inflation, are indeed consistent with the COBE/DMR four years data (Bennet et al., 1996). It is worth remembering that the analysis of these data, based on the assumption of a flat universe, is completely insensitive to the chemistry of the universe. It seems difficult to reconcile the bulk of the observational data (CMB anisotropy, bulk flows, galaxy correlation function, etc.) with a model which is not dynamically dominated by cold dark matter (CDM). However, it does not seems probable that CDM can provide the closure density: if this were the case, the universe would probably be more inhomogeneous than observed on small scales. The excess power on these scales can be reduced, for example, by considering a low density ($\Omega_0 \sim 0.2$) CDM dominated model, which is flat because of a suitable cosmological constant, or a mixture of cold and hot dark matter, i.e. mixed dark matter (MDM) models. In this paper we will focus on the latter scenario. However, just because of the power reduction on small scales, in a MDM model structure formation tends to be a too recent process. This difficulty can be alleviated by considering initial conditions that are not exactly scale invariant. For example, it has been shown that the abundance of rich cluster in MDM models can be better reconciled with the X-ray luminosity function by assuming initial "blue" power spectra, i.e. $P(k) = Ak^n$

with $n \geq 1$ (Lucchin et al. 1996). Blue power spectra could overproduce small scale CMB anisotropy. However, a possible late reheating of the intergalactic medium could have controlled the level of anisotropy at or below the degree angular scale. If and when the universe underwent through a phase of early reionization of the intergalactic medium is an interesting and still open question, although from the Gunn and Peterson (1965) test we know that the universe must have been highly reionized at redshift $z \leq 5$, and the presence of heavy elements in the intracluster gas suggest that a considerable energy release occurred during the earliest stages of galaxy formation and evolution. The recent detections of cosmic microwave background (CMB) anisotropy at degree angular scales provide a new and powerful way for investigating this issue. In fact, the level of detected anisotropies at these scales can in principle discriminate among different assumptions for the thermal history of the universe. Also, using large and intermediate angular scales measurements increases the lever arm for determining the primordial spectral index. A definitive answer to these and other open questions will come when space missions (e.g. COBRAS/SAMBA and MAP) will provide a robust and definitive picture of the intermediate angular scale anisotropy. Meanwhile, the number of experiments reporting detections of anisotropy at degree angular scales has increased up to a couple of tens (see Table I below). Because of their sub-degree angular resolution, these experiments are quite effective in testing different reionization histories. So, the goal of this paper is to discuss if these anisotropy data, together with COBE/DMR, discriminate among different assumptions for the primordial spectral index n and for the thermal history of the universe.

2. Theoretical calculations

We consider a flat universe ($\Omega_0 = 1$) composed by baryons ($0.03 \leq \Omega_b \leq 0.07$), cold dark matter ($\Omega_{CDM} = 1 - \Omega_b - \Omega_\nu$), one family of massive neutrinos ($\Omega_\nu = 0.3$), photons

and two families of massless neutrinos. For age considerations we fix $H_0 = 50km\ s^{-1}/Mpc$, i.e. $h = 0.5$. The basic equations for describing the time evolution of density fluctuations in these different cosmic components have been already derived (Peebles 1981, Peebles 1982a, Peebles 1982b). In Fourier space, they are:

$$\dot{\mathcal{G}} + i\frac{k\mu}{a}\frac{p}{E}\mathcal{G} = \frac{1}{4}\Phi \tag{1}$$

$$\dot{I}_\nu + i\frac{k\mu}{a}I_\nu = \Phi \tag{2}$$

$$\begin{pmatrix} \dot{I}_\gamma \\ \dot{Q}_\gamma \end{pmatrix} + i\frac{k\mu}{a}\begin{pmatrix} I_\gamma \\ Q_\gamma \end{pmatrix} = \Phi\begin{pmatrix} 1 \\ 0 \end{pmatrix} - \sigma_{_T} n_e \left\{ \mathcal{V} + 4i\mu v \begin{pmatrix} 1 \\ 0 \end{pmatrix} - \begin{pmatrix} I_\gamma \\ Q_\gamma \end{pmatrix} \right\} \tag{3}$$

$$\mathcal{V} = \frac{3}{16}\int_{-1}^{1} \begin{pmatrix} 3-\mu'^2-\mu^2+3\mu^2\mu'^2 & 1-\mu'^2-3\mu^2\left(1-\mu'^2\right) \\ 1-3\mu'^2-\mu^2+3\mu^2\mu'^2 & 3-3\mu'^2-3\mu^2\left(1-\mu'^2\right) \end{pmatrix} \begin{pmatrix} I_\gamma \\ Q_\gamma \end{pmatrix} d\mu'$$

$$\ddot{h} + 2\frac{\dot{a}}{a}\dot{h} = 8\pi G\left(\rho_{_B}\delta_{_B} + \rho_{_{CDM}}\delta_{_{CDM}} + 2\rho_\gamma\delta_\gamma + 2\rho_\nu\delta_\nu + 2\rho_{\nu m}\Delta_{\nu m}\right) \tag{4}$$

$$\dot{h}_{33} - \dot{h} = \frac{16\pi G a}{k}\left(\rho_{_B} v + \rho_{\nu m} f_{\nu m} + \rho_\gamma f_\gamma + \rho_\nu f_\nu\right) \tag{5}$$

$$\dot{\delta}_{_B} = \frac{\dot{h}}{2} - i\frac{kv}{a} \tag{6}$$

$$\dot{v} + H(t)v = \sigma_{_T} n_e\left(f_\gamma - \frac{4}{3}v\right) \tag{7}$$

$$\dot{\delta}_{_{CDM}} = \frac{\dot{h}}{2} \tag{8}$$

where $\Phi = (1-\mu^2)\,\dot{h} - (1-3\mu^2)\,\dot{h}_{33}$. Eq.(1) describes the time evolution of the (Fourier transformed) fluctuation in the phase space distribution of massive neutrinos: $\delta\mathcal{F} \equiv Y\mathcal{G}$, where $Y = ye^y(e^y+1)^{-2}$, $y \equiv p/T_\nu$ is the ratio between the neutrino momentum $p = \sqrt{E^2 - m_\nu}$ and the neutrino temperature (we use natural units), proportional to the CMB temperature, $T_\nu = (4/11)^{1/3}T_\gamma$. The massive neutrino background density is then $\rho_{\nu m}(t) = N_{\nu m}\pi^{-2}T_\nu^4(t)\psi^{-1}$ where $\psi = \int_0^\infty dy\, y^2\epsilon\,(e^y+1)^{-1}$, $N_{\nu m}$ is the number of neutrino families with a non vanishing rest mass ($N_{\nu m} = 1$ in our case), $\epsilon = E/T_\nu$, and each flavour state has two helicity states. We expand $\mathcal{G}$ in Legendre polynomials,

$\mathcal{G} = \sum_{\ell=0}^{40} g_\ell P_\ell(\mu)$, and transform Eq.(1) in a set of coupled differential equations for the multipoles g_ℓ (see e.g. Bonometto et al. 1983). The massive neutrino density contrast reads $\delta_{\nu m}(k,t) = \psi^{-1} \int dy\, y^2 \epsilon Y g_0$ while $\Delta_{\nu m} = \psi^{-1} \int dy\, y^2 [y^2 + 1/2(m_\nu/T_\nu)^2] \epsilon^{-1} Y g_0$. For $\epsilon \simeq y$ and $\epsilon \simeq m_\nu$, we have $\Delta_{\nu m} \simeq \delta_{\nu m}$ and $\Delta_{\nu m} = \delta_{\nu m}/2$, respectively. Finally, $f_{\nu m} = \psi^{-1} \int dy y^3 Y g_1$. The integrals in y-space giving $\rho_{\nu m}$, $\Delta_{\nu m}$, $\delta_{\nu m}$ and $f_{\nu m}$ are performed numerically with a 16 points Gauss-Laguerre integration method.

Eq.(2) describes massless neutrinos, and it is obtained by integrating in y- space Eq. (1) in the ultra-relativistic limit ($\epsilon \simeq y$): $I_\nu = 4\mathcal{G}$. Again we expand I_ν in Legendre polynomials, $I_\nu = \sum_{\ell=0}^{40} s_\ell P_\ell(\mu)$ and transform Eq. (2) in a set of 40 coupled differential equations. The density fluctuations of massless neutrinos is $\delta_\nu = s_0$, while $f_\nu = s_1/3$. We numerically follow the evolution of fluctuations in this component only when the perturbation proper wavelength is larger than one tenth of the horizon. Afterwards, free streaming rapidly damps fluctuations in this hot component.

Eq.(3) describes fluctuations in the I and Q Stokes parameters of the CMB (see e.g. Melchiorri A. & Vittorio, 1996) and differs from Eq. (2) because of the collisional term, proportional to the Thomson cross section, σ_T, and to the electronic number density, n_e. The latter is evaluated assuming a standard recombination history (Jones & Wyse 1984), with a helium mass fraction $Y_{He} = 0.23$. We expand I_γ and Q_γ in Legendre polinomials: $I_\gamma = \sum_l \sigma_l P_l$ and $Q_\gamma = \sum_l q_l P_l$. The number of harmonics is automatically increased up to $\ell \leq 5000$ for $k \leq 1 Mpc^{-1}$.

The correlation function (acf) of the temperature fluctuations can be written as

$$C(\alpha, \theta_B) = \frac{1}{4\pi} \sum_{\ell=2}^{\infty} (2\ell+1) C_\ell P_\ell(\cos\alpha) \exp[-(\ell+1/2)^2 \theta_B^2] \tag{9}$$

where θ_B is the dispersion of a Gaussian approximating the angular response of the beam,

and

$$C_\ell = \frac{\mathcal{A}^2}{32\pi^2}\frac{A_{COBE}}{(2\ell+1)^2}\int \mathrm{d}k\ k^{2+n}|\sigma_\ell(|\vec{k}|)|^2, \qquad (10).$$

We define the parameter $\mathcal{A}^2 \equiv A/A_{COBE}$ as the amplitude A of the power spectrum (considered as a free parameter) in units of A_{COBE}, the amplitude needed to reproduce $C(0^o, 4^o.24) = (29\mu K)^2$, as observed by COBE-DMR (Bennet et al., 1996).

Performing the integral in Eq.(10) with high accuracy at high ℓ's requires a very good sampling of the σ_ℓ's in k-space, and this is a heavy computational task. To avoid this problem we sample the interval $-5 < log_{10}k < 0$ with a step $\Delta log_{10}k = 0.01$, we evaluate the integral in Eq.(10), and we use a smoothing algorithm to suppress the high frequency, sample noise. The C_ℓ's obtained in this way differ from those obtained with a much denser k-space sampling ($\Delta log_{10}k = 0.001$) by only a fraction of percent up to $\ell \leq 2000$.

The time evolution of the baryon and CDM density contrasts and of the baryon peculiar velocity are described by Eq.(6), (8) and (7) respectively. The system is closed by Eq.(4) and (5) describing the field equations for the trace and the $3-3$ component of the metric perturbation tensor.

We numerically integrate the previous equations from redshift $z = 10^7$ up to the present. In the following we will also assume that the universe reionized instantaneously at redshift $z_{rh} << 1000$, and remained completely reionized up to the present. Because of the low baryonic abundance, we need reionization at high redshifts in order to substantially suppress the anisotropy at degree scales. For $\Omega_b = 0.05$ and $z_{rh} \leq 70$, there is a probability lower than 50 % for a photon to scatter against a free electron at $z < z_{rh}$.

3. Data analysis

We have selected a set of 20 different anisotropy detections obtained by different experiments, or by the same experiment with different window functions and/or at different frequencies. For each detection, labeled by the index j, we report in Table 1 the detected mean square anisotropy, $\Delta_j^{(exp)}$, and the corresponding 1–σ error, $\Sigma_j^{(exp)}$. In our error estimates, the calibration error was added in quadrature to the statistical error. When not explicitly given, we estimated the mean square anisotropy as follows: $\Delta_j^{(exp)} = Var[\{\Delta T_i\}_j] - \sigma_j^2$, where $\{\Delta T_i\}_j$ are the published anisotropy data of the j-th experiment, $Var[\{\Delta T_i\}_j]$ is the variance of the data points, and σ_j^2 is the mean square value of the instrumental noise.

Theoretically, the mean (over the ensemble) squared anisotropy is given by a weighted sum of the C_ℓ's:

$$[\Delta_j^{(th)}] = \frac{1}{4\pi}\sum_\ell (2\ell+1) C_\ell W_{\ell,j} = \frac{\overline{C_{\ell_{eff}}}}{4\pi}\sum_\ell (2\ell+1) W_{\ell,j} \tag{13}$$

where the windows function $W_{\ell,j}$ contains all the experimental details (chop, modulation, beam ,etc.), and $\overline{C_{\ell_{eff}}}$ is the mean value of the C_ℓ's over the window function. The effective multipole number $\ell_{eff,j}$ is defined as follows:

$$\ell_{eff,j} = \sum \ell(2\ell+1) C_\ell W_{\ell,j} / \sum (2\ell+1) C_\ell W_{\ell,j}$$

and is listed in Table I for a scale invariant model without reionization. Although in principle model dependent, the values of $\ell_{eff,j}$ are quite stable because of the narrowness in ℓ space of the window functions.

Using numerical simulations, which take into account scan strategy and experimental noise, we verify that the expected distribution for $\Delta_j^{(exp)}$ is well approximated by a gaussian,

with mean $\Delta_j^{(th)}$ and a cosmic/sampling variance

$$\Sigma_j^{(th)} = \frac{1}{f_j}\frac{1}{8\pi^2}\sum_\ell (2\ell+1)W_{\ell,j}^2 C_\ell^2 \tag{14}$$

Here f_j represents the fraction of the sky sampled by each experiment and it is also listed in Table I.

Given the Gaussian distribution of $\Delta_j^{(exp)}$, we compute the likelihood of the 20 (assumed independent) CMB anisotropy detections as follows:

$$\mathcal{L}(\mathcal{A}, n, z_{rh}) = \prod_j \frac{1}{\sqrt{2\pi[\mathcal{A}^4(\Delta_j^{(th)})^2 + \Sigma_j^2]}} \exp\{-\frac{1}{2}\frac{[\Delta_j^{(exp)} - \mathcal{A}^2\Delta_j^{(th)}]^2}{\mathcal{A}^4(\Delta_j^{(th)})^2 + \Sigma_j^2}\} \tag{15}$$

As already stated, this is a function of three parameters: the amplitude $\mathcal{A}$, the spectral index n and the reionization redshift z_{rh}.

For each pair $n - z_{rh}$ we select the value $\mathcal{A}_{max}$ which maximizes the Likelihood (isolevels of $\mathcal{A}_{max}$ are shown in Fig.1 for $\Omega_b = 0.03, 0.05, 0.07$, respectively). The results of our theoretical calculation are shown in Fig.2a, where we plot the C_ℓ's for few models, each of them normalized with its own $\mathcal{A}_{max}$. Our results show that the difference between a pure CDM and a MDM ($\Omega_\nu = 0.3$) models, normalized with the same $\mathcal{A}_{max}$ is very tiny, $\leq 2\%$ up to $\ell \leq 300$ and $\leq 8\%$ up to $\ell \leq 800$ (de Gasperis et al., 1995, Gates, Dodelson and Stebbins 1995, Ma & Bertschinger 1995). So we will make hereafter the assumption that the anisotropy pattern does not depend on Ω_ν, at least for $\Omega_\nu \leq 0.3$. This generalizes our assumption that the CMB anisotropy depends only upon three independent variables: $\mathcal{A}$, n and z_{rh}. For the models shown in Fig.1a we also plot the band-power estimate for the j-th experiment $\overline{C_{\ell_{eff}}} = 4\pi\Delta_j^{(exp)} / \sum (2\ell+1)W_{\ell,j}$ and in Fig.1b the corresponding window functions, $W_{\ell,j}$.

The 2-D, conditional distribution $L(n, z_r|A_{max}) \equiv \mathcal{L}(\mathcal{A}_{max}, n, z_{rh})$ has a quite distinctive peak at $n = 1.24$ and $z_{rh} = 20$. A P-confidence level contour in the $n - z_{rh}$ is obtained cutting the L distribution with the isolevel L_P, and by requiring that the volume below the

surface inside L_P is a fraction P of the total volume. In Fig.3 we plot the L_{68} and the L_{95} contours, again for $\Omega_b = 0.03, 0.05$ and 0.07, respectively (we actually sampled a region of the $n - z_{rh}$ plane much larger than shown in Figure).

It is clear that the considered data set identifies a preferred region of the $n - z_{rh}$ space. The shape of the confidence contours can be understood by noting that increasing n would overproduce anisotropies: a corresponding increase in z_{rh} is thus required to damp the fluctuations to a level compatible with observations. On the other hand, if Ω_b is increased, the optical depth increases, thus requiring a lower reionization redshift to produce the detected level of degree-scale anisotropy. This effect dominates over the smaller increase of primary CMB anisotropies.

The simple analysis carried out here does not take into account details on the scan pattern and/or the beam profile. Moreover, we know that the published error bars could not account properly for correlated errors or other more subtle effects. In order to test the significance of our analysis and its robustness against the published estimates for the experimental errors, we take a drastic point of view: we consider the best fit model ($n = 1.24$, $z_{rh} = 20$) normalized to COBE/DMR (i.e. we fix $\mathcal{A} = 1$). For each degree–scale data point we compute the difference between the measured value and the value expected from the theory. We then associate to each data point a 1–σ error bar equal to the root mean square of these 19 differences (instead of the published error bars). The corresponding results of the likelihood analysis are in very good agreement with what is found using the appropriate errors: $n > 1$ is slightly better, especially if the reionization redshift is increased. So we do believe that our results are little affected by possible correlations in the errors and/or systematics.

4. Conclusions

Our main conclusions, derived from Fig.3, are as follows.

1. The conditional Likelihood shows a maximum for $n = 1.24$ and $z_{rh} = 20$, for $0.03 \leq \Omega_b \leq 0.07$, i.e. for baryonic abundances consistent with primordial nucleosynthesis. We have checked the stability of this result by applying a jack-knife analysis to the considered data set, and we have seen that the results are reasonably stable: the best model has always $n = 1.24(\pm 0.02)$ and $z_{rh} = 20(\pm 10)$, unless COBE data are excluded (in that case $n = 1.40$ and $z_{rh} = 20$).

2. The 95% confidence contours in the $n - z_{rh}$ plane include a wide range of parameters combinations. This means that the presently available data set is not sensitive enough to produce "precise" determinations for n and z_{rh}; systematic and statistical errors in the different experiments are still significant.

3. If we exclude an early reionization of the intergalactic medium ($z_{rh} = 0$) we get the following 95% confidence level estimates for the spectral index: $1.02 \leq n \leq 1.28$ ($\Omega_b = 0.03$); $1.00 \leq n \leq 1.26$ ($\Omega_b = 0.05$); $0.96 \leq n \leq 1.24$ ($\Omega_b = 0.07$). This has to be compared to the results from COBE-DMR alone: $n = (1.3 \pm 0.3)$, at the 68% confidence level (Bennet et al., 1996). So, in spite of their still low signal to noise ratio, the degree scale experiments already allow to better constrain the spectral index, although still at the 10% level. Note that the "standard", flat model with no reionization is close but not always inside the 95% confidence contour. However, this result is determined mainly by the Saskatoon experiment. In fact, we tested the stability of our results by repeating the analysis several times, excluding one experiment at the time. If we do not consider reionization, the 95% C.L. interval $1.00 \leq n \leq 1.26$ does not change more than a few % excluding either Argo, CAT, MAX, MSAM, South Pole or Tenerife. The lower limit drops to $0.86 \leq n$ if the Saskatoon data are excluded, while the upper limit raises to $n \leq 1.76$ if

the COBE data are excluded. This test also shows that neglecting the correlation due to overlapping sky coverage (e.g. Tenerife and COBE, and/or MSAM and Saskatoon) does not change significantly the results of our analysis.

4. For scale invariant models with no reionization, the height of the first "Doppler" peak occurs at $\ell \simeq 220$ and is a factor of $\simeq 5.6$ higher than the Sachs-Wolfe plateau at low ℓ's. For $n = 1.2$ the peak amplitude is roughly a factor 1.5 higher than in the scale-invariant case. A complete reionization from $z_{rh} \simeq 20$ up to the present suppress the peak by roughly 20%. Altogether, a model with $n = 1.2$ and $z_{rh} = 20$ has a Doppler peak a factor of 2 higher than in the standard scale invariant case without reheating. So our analysis confirms that a Doppler peak in the C_ℓ spectrum centered at ~ 200 is perfectly consistent with the data.

All the models we have worked with have, as stated above, $h = 0.5$. In flat models with vanishing cosmological constant we can expect $0.4 \leq h \leq 0.65$ from the estimated age of globular clusters (Kolb E.W. & Turner M.S.). Varying h modifies the amplitude and position of the acoustic peaks in the radiation power spectrum. However, we have verified that, in the region of the spectrum probed by current anisotropy experiments, 20% variations of the Hubble constant yeld modifications in the spectrum very similar to those obtained varying Ω_b between 0.03 and 0.07. Also, we did not consider tensor modes in our analysis, as they are expected to be of negligible amplitude for $n > 1$ (Steinhardt P.J. 1995). We will address this issue in a forthcoming paper.

REFERENCES

Abbot L.F. and Wise M.B., 1984, ApJ, 282, L47.

Bennet C.L., et al. 1994, ApJ, 436, 423.

Bennet C.L., et al. 1996, ApJ, 464, 1.

Bonometto et al. ,1983 , A&A, 123, 118B.

Cheng E.S., et al.1994, ApJ, 422, L40.

de Bernardis P., et al. 1994, ApJ, 422, L33.

de Gasperis, G., Muciaccia, P.F. and Vittorio, N. 1995, ApJ, 439, 1.

Dragovan M., et al. 1993, ApJ, 427, L67.

Gates, Dodelson and Stebbins, astro-ph/9509147, 1995

Gundersen J.O., et al. 1993, ApJ, 413, L1.

Gunn J.E., Peterson B.A., 1965, ApJ, 142, 1633.

Hancock S., et al., 1994, Nature, 367, 333.

Jones & Wyse 1985 A&A, 149, 144J.

Kolb & Turner, 1990, The Early Universe, Addison-Wesley, NY.

Lucchin F. et al. 1996, preprint astro-ph 9504028.

Ma C.P. & Bertschinger E., 1995, Ap.J., 455, 7.

Masi S., et al. 1996, ApJ, 463, L47.

Melchiorri A. and Vittorio N., 1996 in preparation

Melchiorri A., Balbi A., de Bernardis P., De Gasperis G. and Vittorio N., 1996 in preparation

Netterfield et al., 1996, in press, astro-ph 9601197

Peebles P.J.E. 1982A, ApJ, 263L , 1P.

Peebles P.J.E. 1982B, ApJ, 259 , 442P.

Peebles P.J.E. 1981, ApJ, 248 , 885.

Scaramella, R. & Vittorio, N., 1993, MNRAS, 263 , L17.

Sachs R.K., Wolfe A.M., 1967, ApJ, 147, 73.

Scott P.F. et al., 1996, ApJ, 461, L1.

Smoot G., et al. 1992, ApJ, 396, L1 (DMR92).

Steinhardt P.J. astro-ph 9502024.

Tanaka S.T. et al. 1996, ApJ, in press, astro-ph 9512067

Fig. 1.— Isolevels of the normalization amplitude $\mathcal{A}_{max}$, which maximizes the combined likelihood $\mathcal{L}(\mathcal{A}, n, z_{rh})$.

Fig. 2.— Power spectra of CMB anisotropies for different combinations of spectral index and reionization redshift (panel a). The data points are derived from the experiments listed in Table 1. In panel b we plot the corresponding filter functions.

Fig. 3.— Confidence level (68 and 95%) regions for the spectral index n and the reionization redshift z_{rh}. The black square marks the position of the model featuring the maximum likelihood.

TABLE 1

CMB Anisotropy Detections Used in the Analysis

experiment	ref.	$\Delta T^2(\mu K^2)$	68%+, (μK^2)	68%-, (μK^2)	sky coverage	ℓ_{eff}
COBE	1	841	58	57	0.6580	5.8
Tenerife	2	1770	840	670	0.0124	20.1
South Pole Q	3	480	470	160	0.0005	49.4
South Pole K	4	2040	2330	790	0.0005	65.7
Python	5	1940	1890	490	0.0006	129.0
ARGO Hercules	6	360	170	140	0.0024	118.9
ARGO Aries	7	580	150	130	0.0055	118.9
MAX HR	8	2430	1850	1020	0.0002	162.0
MAX PH	9	5960	5080	2190	0.0002	162.0
MAX GUM	10	6580	4450	2320	0.0002	162.0
MAX ID	11	4960	5690	2330	0.0002	162.0
MAX SH	12	5740	6280	2900	0.0002	162.0
MSAM 3F	13	4680	4200	2450	0.0007	181.3
Saskatoon	14	1990	950	630	0.0037	99.9
Saskatoon	15	4490	1690	1360	0.0037	175.4
Saskatoon	16	6930	2770	2140	0.0037	235.2
Saskatoon	17	6980	3030	2310	0.0037	283.2
Saskatoon	18	4730	3380	3190	0.0037	347.8
CAT 1	19	1180	720	520	0.0001	414.9
CAT 2	20	760	760	360	0.0001	579.7

References.— (1) Bennet et al., 1996; (2) Hancock et al. 1994; (3,4) Gundersen et al. 1994; (5) Dragovan et al. 1994; (6) de Bernardis et al. 1994; (7) Masi et al. 1996; (8,9,10,11,12) Tanaka et al. 1996; (13) Cheng et al. 1994; (14, 15, 16, 17, 18) Netterfield et al. 1996; (19, 20) Scott et al. 1996

Fig.1

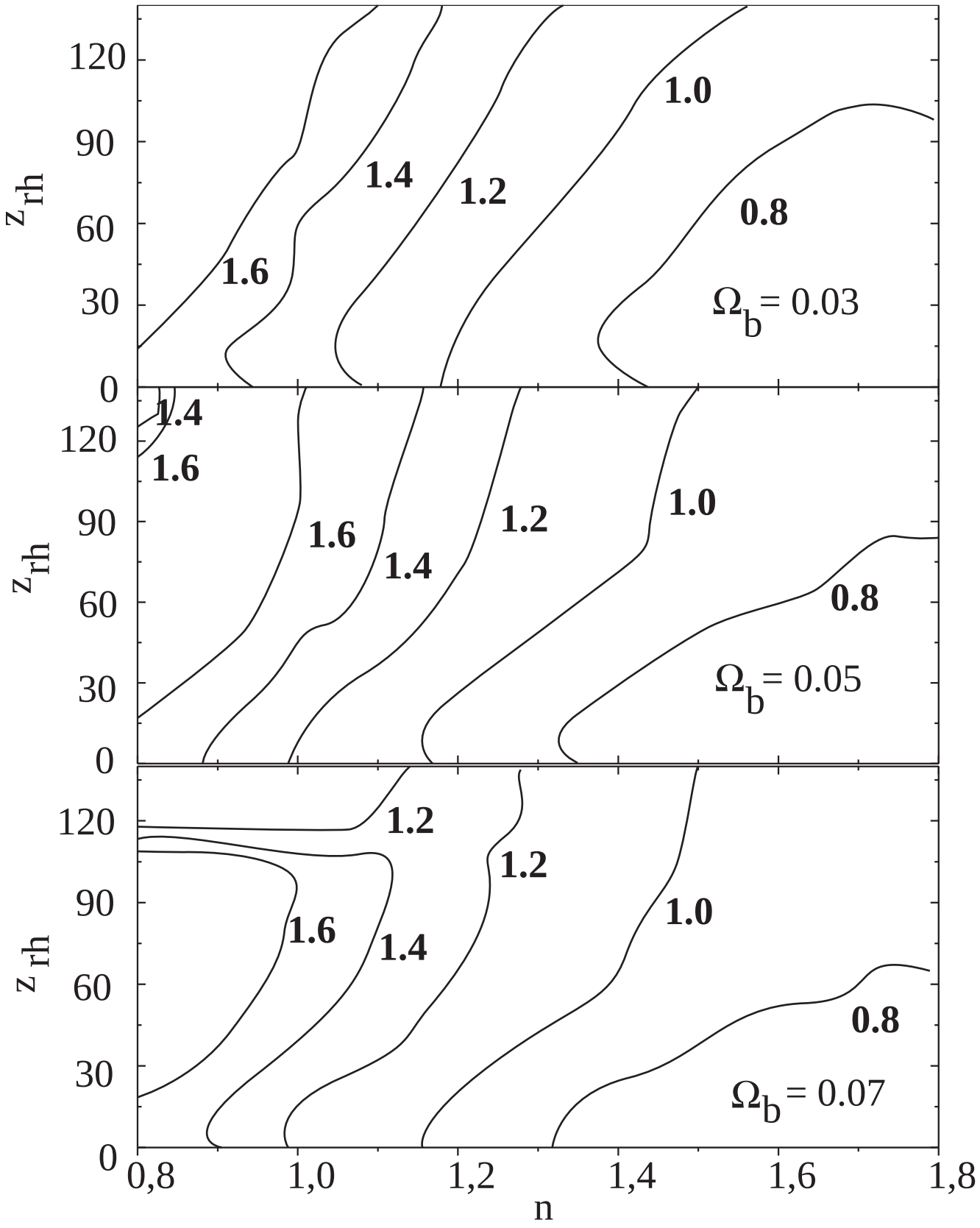
Normalization amplitude
120
90
60
30
0
z rh
1.6
1.4
1.2
1.0
0.8
Ω b = 0.03
1.4
1.6
1.6
1.4
1.2
1.0
0.8
Ω b = 0.05
1.2
1.2
1.6
1.4
1.0
0.8
Ω b = 0.07
0,8
1,0
1,2
1,4
1,6
1,8
n

Fig.2A

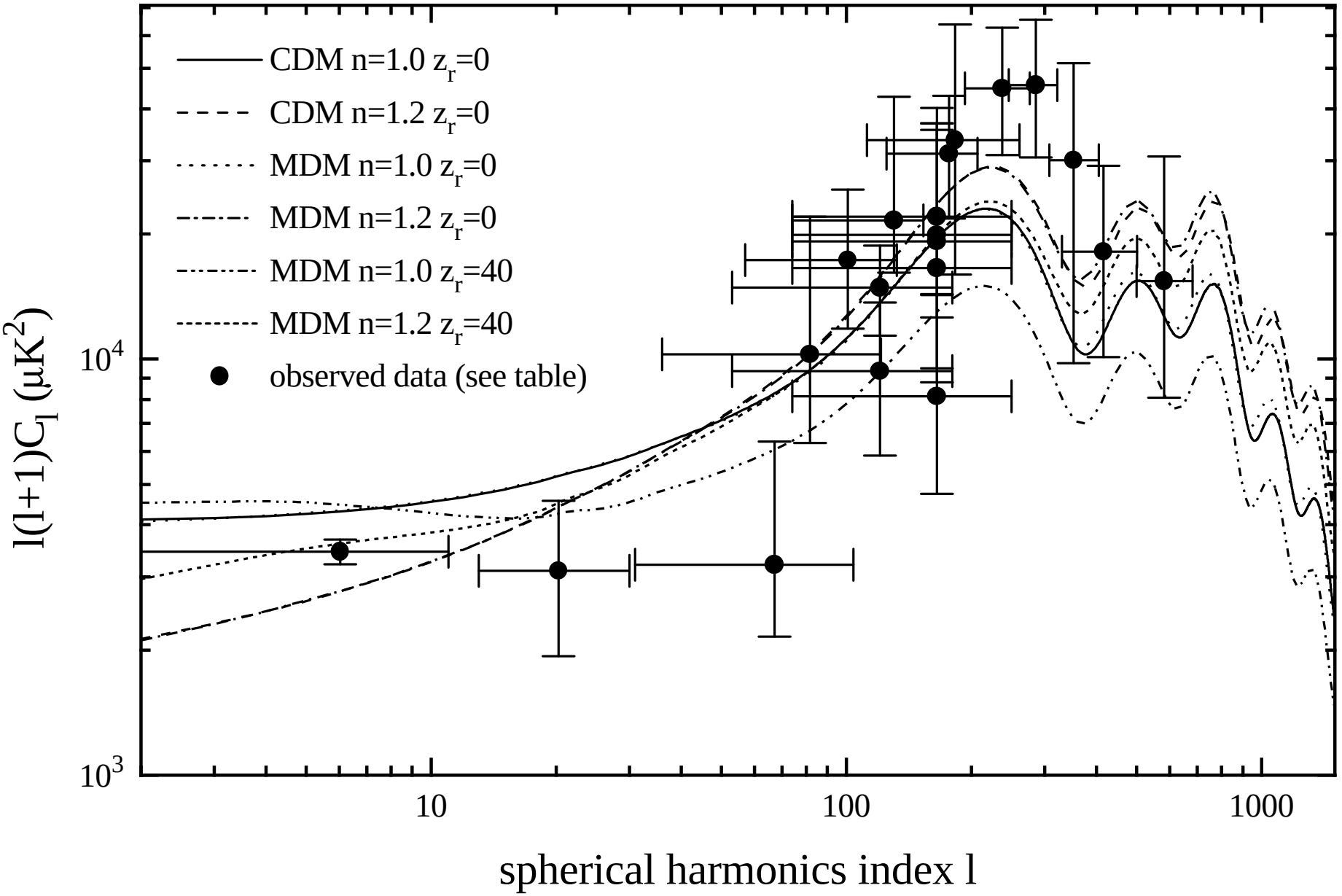
CDM n=1.0 z_r=0
CDM n=1.2 z_r=0
MDM n=1.0 z_r=0
MDM n=1.2 z_r=0
MDM n=1.0 z_r=40
MDM n=1.2 z_r=40
observed data (see table)
l(l+1)C_l (μK^2)
10^4
10^3
10
100
1000
spherical harmonics index l

Fig.2B

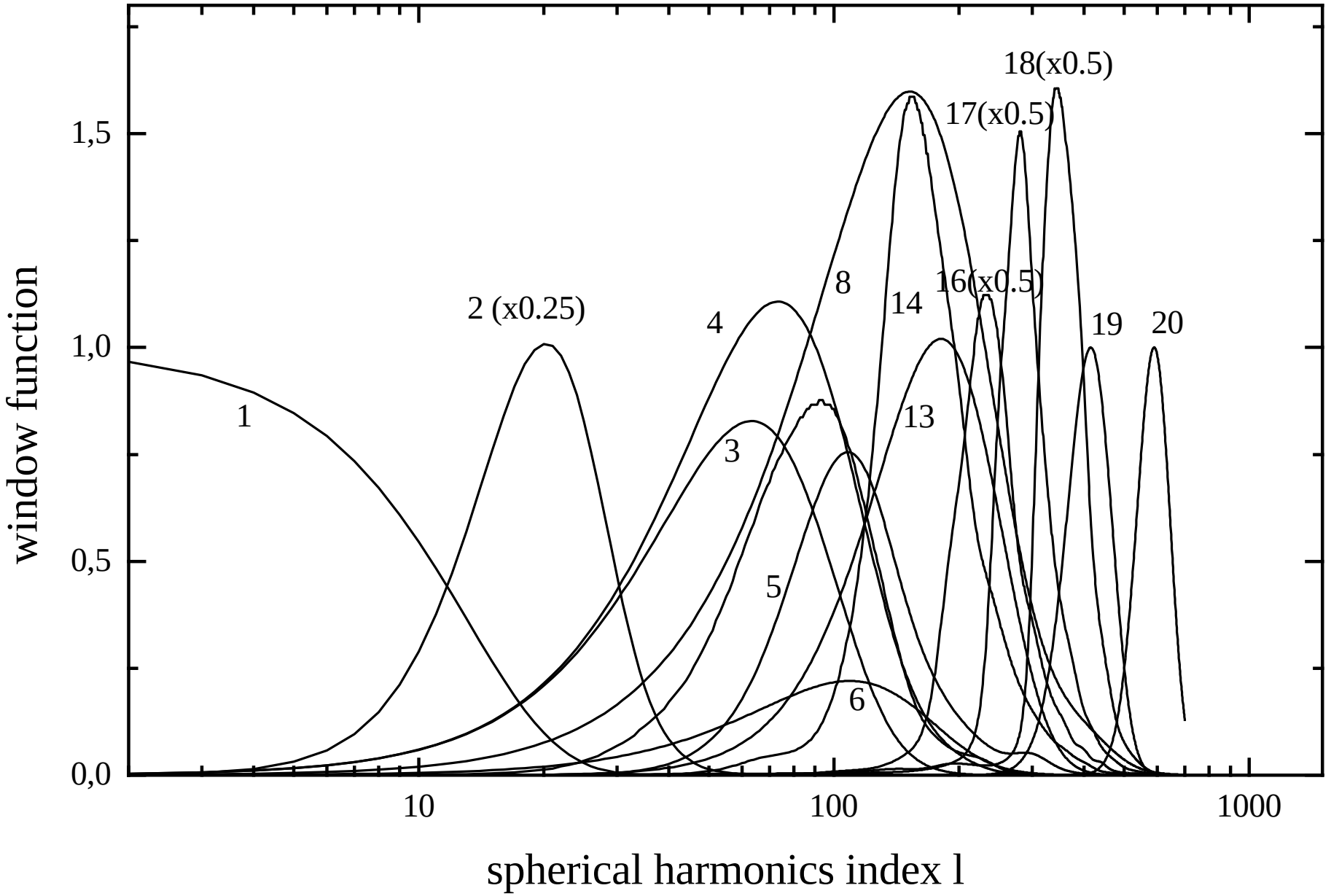
window function
1,5
1,0
0,5
0,0
10
100
1000
spherical harmonics index l
1
2 (x0.25)
3
4
5
6
8
13
14
16(x0.5)
17(x0.5)
18(x0.5)
19
20

Fig.3 Likelihood contours